# Pion, kaon, proton and anti-proton transverse momentum distributions from p+p and d+Au collisions at $\sqrt{s_{NN}} = 200$ GeV

J. Adams,[3] C. Adler,[12] M.M. Aggarwal,[25] Z. Ahammed,[38] J. Amonett,[17] B.D. Anderson,[17] M. Anderson,[5] D. Arkhipkin,[11] G.S. Averichev,[10] S.K. Badyal,[16] J. Balewski,[13] O. Barannikova,[28,10] L.S. Barnby,[17] J. Baudot,[15] S. Bekele,[24] V.V. Belaga,[10] R. Bellwied,[41] J. Berger,[12] B.I. Bezverkhny,[43] S. Bhardwaj,[29] P. Bhaskar,[38] A.K. Bhati,[25] H. Bichsel,[40] A. Billmeier,[41] L.C. Bland,[2] C.O. Blyth,[3] B.E. Bonner,[30] M. Botje,[23] A. Boucham,[34] A. Brandin,[21] A. Bravar,[2] R.V. Cadman,[1] X.Z. Cai,[33] H. Caines,[43] M. Calderón de la Barca Sánchez,[2] J. Carroll,[18] J. Castillo,[18] M. Castro,[41] D. Cebra,[5] P. Chaloupka,[9] S. Chattopadhyay,[38] H.F. Chen,[32] Y. Chen,[6] S.P. Chernenko,[10] M. Cherney,[8] A. Chikanian,[43] B. Choi,[36] W. Christie,[2] J.P. Coffin,[15] T.M. Cormier,[41] J.G. Cramer,[40] H.J. Crawford,[4] D. Das,[38] S. Das,[38] A.A. Derevschikov,[27] L. Didenko,[2] T. Dietel,[12] X. Dong,[32,18] J.E. Draper,[5] F. Du,[43] A.K. Dubey,[14] V.B. Dunin,[10] J.C. Dunlop,[2] M.R. Dutta Majumdar,[38] V. Eckardt,[19] L.G. Efimov,[10] V. Emelianov,[21] J. Engelage,[4] G. Eppley,[30] B. Erazmus,[34] M. Estienne,[34] P. Fachini,[2] V. Faine,[2] J. Faivre,[15] R. Fatemi,[13] K. Filimonov,[18] P. Filip,[9] E. Finch,[43] Y. Fisyak,[2] D. Flierl,[12] K.J. Foley,[2] J. Fu,[42] C.A. Gagliardi,[35] M.S. Ganti,[38] T.D. Gutierrez,[5] N. Gagunashvili,[10] J. Gans,[43] L. Gaudichet,[34] M. Germain,[15] F. Geurts,[30] V. Ghazikhanian,[6] P. Ghosh,[38] J.E. Gonzalez,[6] O. Grachov,[41] V. Grigoriev,[21] S. Gronstal,[8] D. Grosnick,[37] M. Guedon,[15] S.M. Guertin,[6] A. Gupta,[16] E. Gushin,[21] T.J. Hallman,[2] D. Hardtke,[18] J.W. Harris,[43] M. Heinz,[43] T.W. Henry,[35] S. Heppelmann,[26] T. Herston,[28] B. Hippolyte,[43] A. Hirsch,[28] E. Hjort,[18] G.W. Hoffmann,[36] M. Horsley,[43] H.Z. Huang,[6] S.L. Huang,[32] T.J. Humanic,[24] G. Igo,[6] A. Ishihara,[36] P. Jacobs,[18] W.W. Jacobs,[13] M. Janik,[39] I. Johnson,[18] P.G. Jones,[3] E.G. Judd,[4] S. Kabana,[43] M. Kaneta,[18] M. Kaplan,[7] D. Keane,[17] J. Kiryluk,[6] A. Kisiel,[39] J. Klay,[18] S.R. Klein,[18] A. Klyachko,[13] D.D. Koetke,[37] T. Kollegger,[12] A.S. Konstantinov,[27] M. Kopytine,[17] L. Kotchenda,[21] A.D. Kovalenko,[10] M. Kramer,[22] P. Kravtsov,[21] K. Krueger,[1] C. Kuhn,[15] A.I. Kulikov,[10] A. Kumar,[25] G.J. Kunde,[43] C.L. Kunz,[7] R.Kh. Kutuev,[11] A.A. Kuznetsov,[10] M.A.C. Lamont,[3] J.M. Landgraf,[2] S. Lange,[12] C.P. Lansdell,[36] B. Lasiuk,[43] F. Laue,[2] J. Lauret,[2] A. Lebedev,[2] R. Lednický,[10] V.M. Leontiev,[27] M.J. LeVine,[2] C. Li,[32] Q. Li,[41] S.J. Lindenbaum,[22] M.A. Lisa,[24] F. Liu,[42] L. Liu,[42] Z. Liu,[42] Q.J. Liu,[40] T. Ljubicic,[2] W.J. Llope,[30] H. Long,[6] R.S. Longacre,[2] M. Lopez-Noriega,[24] W.A. Love,[2] T. Ludlam,[2] D. Lynn,[2] J. Ma,[6] Y.G. Ma,[33] D. Magestro,[24] S. Mahajan,[16] L.K. Mangotra,[16] D.P. Mahapatra,[14] R. Majka,[43] R. Manweiler,[37] S. Margetis,[17] C. Markert,[43] L. Martin,[34] J. Marx,[18] H.S. Matis,[18] Yu.A. Matulenko,[27] T.S. McShane,[8] F. Meissner,[18] Yu. Melnick,[27] A. Meschanin,[27] M. Messer,[2] M.L. Miller,[43] Z. Milosevich,[7] N.G. Minaev,[27] C. Mironov,[17] D. Mishra,[14] J. Mitchell,[30] B. Mohanty,[38] L. Molnar,[28] C.F. Moore,[36] M.J. Mora-Corral,[19] V. Morozov,[18] M.M. de Moura,[41] M.G. Munhoz,[31] B.K. Nandi,[38] S.K. Nayak,[16] T.K. Nayak,[38] J.M. Nelson,[3] P. Nevski,[2] V.A. Nikitin,[11] L.V. Nogach,[27] B. Norman,[17] S.B. Nurushev,[27] G. Odyniec,[18] A. Ogawa,[2] V. Okorokov,[21] M. Oldenburg,[18] D. Olson,[18] G. Paic,[24] S.U. Pandey,[41] S.K. Pal,[38] Y. Panebratsev,[10] S.Y. Panitkin,[2] A.I. Pavlinov,[41] T. Pawlak,[39] V. Perevoztchikov,[2] W. Peryt,[39] V.A. Petrov,[11] S.C. Phatak,[14] R. Picha,[5] M. Planinic,[44] J. Pluta,[39] N. Porile,[28] J. Porter,[2] A.M. Poskanzer,[18] M. Potekhin,[2] E. Potrebenikova,[10] B.V.K.S. Potukuchi,[16] D. Prindle,[40] C. Pruneau,[41] J. Putschke,[19] G. Rai,[18] G. Rakness,[13] R. Raniwala,[29] S. Raniwala,[29] O. Ravel,[34] R.L. Ray,[36] S.V. Razin,[10,13] D. Reichhold,[28] J.G. Reid,[40] G. Renault,[34] F. Retiere,[18] A. Ridiger,[21] H.G. Ritter,[18] J.B. Roberts,[30] O.V. Rogachevski,[10] J.L. Romero,[5] A. Rose,[41] C. Roy,[34] L.J. Ruan,[32,2] R. Sahoo,[14] I. Sakrejda,[18] S. Salur,[43] J. Sandweiss,[43] I. Savin,[11] J. Schambach,[36] R.P. Scharenberg,[28] N. Schmitz,[19] L.S. Schroeder,[18] K. Schweda,[18] J. Seger,[8] D. Seliverstov,[21] P. Seyboth,[19] E. Shahaliev,[10] M. Shao,[32] M. Sharma,[25] K.E. Shestermanov,[27] S.S. Shimanskii,[10] R.N. Singaraju,[38] F. Simon,[19] G. Skoro,[10] N. Smirnov,[43] R. Snellings,[23] G. Sood,[25] P. Sorensen,[6] J. Sowinski,[13] H.M. Spinka,[1] B. Srivastava,[28] S. Stanislaus,[37] R. Stock,[12] A. Stolpovsky,[41] M. Strikhanov,[21] B. Stringfellow,[28] C. Struck,[12] A.A.P. Suaide,[41] E. Sugarbaker,[24] C. Suire,[2] M. Šumbera,[9] B. Surrow,[2] T.J.M. Symons,[18] A. Szanto de Toledo,[31] P. Szarwas,[39] A. Tai,[6] J. Takahashi,[31] A.H. Tang,[2,23] D. Thein,[6] J.H. Thomas,[18] V. Tikhomirov,[21] M. Tokarev,[10] M.B. Tonjes,[20] T.A. Trainor,[40] S. Trentalange,[6] R.E. Tribble,[35] M.D. Trivedi,[38] V. Trofimov,[21] O. Tsai,[6] T. Ullrich,[2] D.G. Underwood,[1] G. Van Buren,[2] A.M. VanderMolen,[20] A.N. Vasiliev,[27] M. Vasiliev,[35] S.E. Vigdor,[13] Y.P. Viyogi,[38] S.A. Voloshin,[41] W. Waggoner,[8] F. Wang,[28] G. Wang,[17] X.L. Wang,[32] Z.M. Wang,[32] H. Ward,[36] J.W. Watson,[17] R. Wells,[24] G.D. Westfall,[20] C. Whitten Jr.,[6] H. Wieman,[18] R. Willson,[24] S.W. Wissink,[13] R. Witt,[43] J. Wood,[6] J. Wu,[32] N. Xu,[18] Z. Xu,[2] Z.Z. Xu,[32] A.E. Yakutin,[27] E. Yamamoto,[18] J. Yang,[6] P. Yepes,[30] V.I. Yurevich,[10] Y.V. Zanevski,[10] I. Zborovský,[9] H. Zhang,[43,2] H.Y. Zhang,[17] W.M. Zhang,[17] Z.P. Zhang,[32] P.A. Żołnierczuk,[13] R. Zoulkarneev,[11] J. Zoulkarneeva,[11] and A.N. Zubarev[10]

(STAR Collaboration),*

[1]*Argonne National Laboratory, Argonne, Illinois 60439*
[2]*Brookhaven National Laboratory, Upton, New York 11973*
[3]*University of Birmingham, Birmingham, United Kingdom*
[4]*University of California, Berkeley, California 94720*
[5]*University of California, Davis, California 95616*
[6]*University of California, Los Angeles, California 90095*
[7]*Carnegie Mellon University, Pittsburgh, Pennsylvania 15213*
[8]*Creighton University, Omaha, Nebraska 68178*
[9]*Nuclear Physics Institute AS CR, Řež/Prague, Czech Republic*
[10]*Laboratory for High Energy (JINR), Dubna, Russia*
[11]*Particle Physics Laboratory (JINR), Dubna, Russia*
[12]*University of Frankfurt, Frankfurt, Germany*
[13]*Indiana University, Bloomington, Indiana 47408*
[14]*Insitute of Physics, Bhubaneswar 751005, India*
[15]*Institut de Recherches Subatomiques, Strasbourg, France*
[16]*University of Jammu, Jammu 180001, India*
[17]*Kent State University, Kent, Ohio 44242*
[18]*Lawrence Berkeley National Laboratory, Berkeley, California 94720*
[19]*Max-Planck-Institut für Physik, Munich, Germany*
[20]*Michigan State University, East Lansing, Michigan 48824*
[21]*Moscow Engineering Physics Institute, Moscow Russia*
[22]*City College of New York, New York City, New York 10031*
[23]*NIKHEF, Amsterdam, The Netherlands*
[24]*Ohio State University, Columbus, Ohio 43210*
[25]*Panjab University, Chandigarh 160014, India*
[26]*Pennsylvania State University, University Park, Pennsylvania 16802*
[27]*Institute of High Energy Physics, Protvino, Russia*
[28]*Purdue University, West Lafayette, Indiana 47907*
[29]*University of Rajasthan, Jaipur 302004, India*
[30]*Rice University, Houston, Texas 77251*
[31]*Universidade de Sao Paulo, Sao Paulo, Brazil*
[32]*University of Science & Technology of China, Anhui 230027, China*
[33]*Shanghai Institute of Nuclear Research, Shanghai 201800, P.R. China*
[34]*SUBATECH, Nantes, France*
[35]*Texas A&M, College Station, Texas 77843*
[36]*University of Texas, Austin, Texas 78712*
[37]*Valparaiso University, Valparaiso, Indiana 46383*
[38]*Variable Energy Cyclotron Centre, Kolkata 700064, India*
[39]*Warsaw University of Technology, Warsaw, Poland*
[40]*University of Washington, Seattle, Washington 98195*
[41]*Wayne State University, Detroit, Michigan 48201*
[42]*Institute of Particle Physics, CCNU (HZNU), Wuhan, 430079 China*
[43]*Yale University, New Haven, Connecticut 06520*
[44]*University of Zagreb, Zagreb, HR-10002, Croatia*

(Dated: September 15, 2003)

Identified mid-rapidity particle spectra of $\pi^{\pm}$, $K^{\pm}$, and $p(\bar{p})$ from 200 GeV p+p and d+Au collisions are reported. A time-of-flight detector based on multi-gap resistive plate chamber technology is used for particle identification. The particle-species dependence of the Cronin effect is observed to be significantly smaller than that at lower energies. The ratio of the nuclear modification factor ($R_{dAu}$) between $(p+\bar{p})$ and charged hadrons ($h$) in the transverse momentum range $1.2 < p_T < 3.0$ GeV/c is measured to be $1.19 \pm 0.05(\text{stat}) \pm 0.03(\text{syst})$ in minimum-bias collisions and shows little centrality dependence. The yield ratio of $(p+\bar{p})/h$ in minimum-bias d+Au collisions is found to be a factor of 2 lower than that in Au+Au collisions, indicating that the Cronin effect alone is not enough to account for the relative baryon enhancement observed in heavy ion collisions at RHIC.

PACS numbers: 25.75.Dw, 13.85.Ni

Suppression of high transverse momentum ($p_T$) hadron production has been observed at RHIC in central Au+Au collisions relative to p+p collisions [1, 2]. This suppression has been interpreted as energy loss of the energetic partons traversing the produced hot and dense medium [3]. At intermediate $p_T$, the degree of suppres-

*URL: `www.star.bnl.gov`

sion depends on particle species. The spectra of baryons (protons and lambdas) are less suppressed than those of mesons (pions, kaons) [4, 5] in the $p_T$ range $2 < p_T < 5$ GeV/c. Hydrodynamics [6, 7], parton coalescence at hadronization [8, 9, 10] and gluon junctions [11] have been suggested as explanations for the observed particle-species dependence.

On the other hand, the hadron $p_T$ spectra have been observed to depend on the target atomic weight ($A$) and the produced particle species in lower energy p+A collisions [12]. This is known as the "Cronin Effect", a generic term for the experimentally observed broadening of the transverse momentum distributions at intermediate $p_T$ in p+A collisions as compared to those in p+p collisions [12, 13, 14]. The effect can be characterized as a dependence of the yield on the target atomic weight as $A^\alpha$. At energies of $\sqrt{s} \simeq 30$ GeV, $\alpha$ depends on $p_T$ and is greater than unity at high $p_T$ [12], indicating an enhancement of the production cross section. The effect has been interpreted as partonic scatterings at the initial impact [13, 14]. At higher energies, multiple parton collisions are possible even in p+p collisions [15]. This combined with the hardening of the spectra with increasing beam energy would reduce the Cronin effect [14]. At sufficiently high beam energy, gluon saturation is expected to result in a relative suppression of hadron yield at high $p_T$ in both p+A and A+A collisions in addition to the enhancement from the Cronin effect [16].

Recent results on inclusive hadron production from d+Au collisions indicate that hadron suppression at intermediate $p_T$ in Au+Au collisions is due to final-state effects [17, 18]. In order to further understand the mechanisms responsible for the particle dependence of $p_T$ spectra in heavy ion collisions, and to separate the effects of initial and final partonic rescatterings, we measured the $p_T$ distributions of $\pi^\pm$, $K^\pm$, $p$ and $\bar{p}$ from 200 GeV d+Au and p+p collisions. In this letter, we discuss the dependence of particle production on $p_T$, collision energy, and target atomic weight.

The detector used for these studies was the Solenoidal Tracker at RHIC (STAR). The main tracking device is the Time Projection Chamber (TPC) which provides momentum information and particle identification for charged particles up to $p_T \sim 1.1$ GeV/c by measuring their ionization energy loss ($dE/dx$) [19]. Detailed descriptions of the TPC and d+Au run conditions have been presented in Ref. [17, 19].

A time-of-flight detector (TOFr) based on multi-gap resistive plate chambers (MRPC) [20] was installed in STAR for the d+Au and p+p runs. It extends particle identification up to $p_T \sim 3$ GeV/c for $p$ and $\bar{p}$. MRPC technology was first developed by the CERN ALICE group [21] to provide a cost-effective solution for large-area time-of-flight coverage. We report the first physics results from detectors based on this new MRPC technology.

TOFr covers $\pi/30$ in azimuth and $-1<\eta<0$ in pseudo-rapidity at a radius of $\sim 220$ cm. It contains 28 MRPC

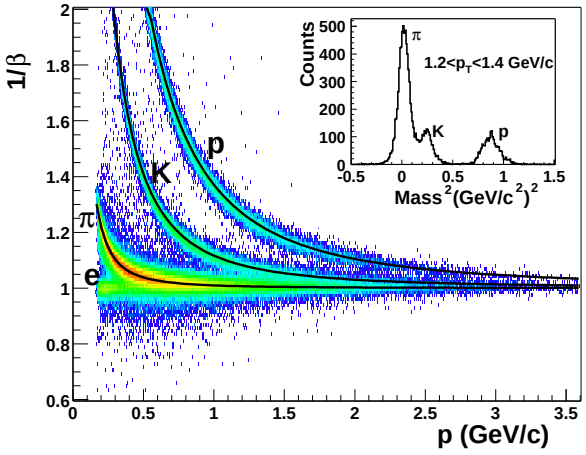


FIG. 1: $1/\beta$ vs. momentum for $\pi^\pm$, $K^\pm$, and $p(\bar{p})$ from 200 GeV d+Au collisions. Separations between pions and kaons, kaons and protons are achieved up to $p_T \simeq 1.6$ and 3.0 GeV/c, respectively. The insert shows $m^2 = p^2(1/\beta^2 - 1)$ for $1.2 < p_T < 1.4$ GeV/c. Clear separation of $\pi$, $K$ and $p$ is seen.

modules. Each module [20] is a stack of resistive glass plates with six uniform gas gaps. High voltage is applied to electrodes on the outer surfaces of the outer plates. A charged particle traversing a module generates avalanches in the gas gaps which are read out by 6 copper pickup pads with pad dimensions of $31.5 \times 63$ mm$^2$. The MRPC modules were operated at 14 kV with a mixture of 95% $C_2H_2F_4$ and 5% iso-butane at 1 atmosphere.

The face of each MRPC module is approximately normal to the straight track trajectory for an interaction at the TPC center. In d+Au collisions, TOFr is situated in the outgoing Au beam direction which is assigned negative $\eta$. Twelve of the 28 modules were instrumented during the 2003 run, corresponding to 0.3% of the TPC acceptance. This analysis used 56 readout channels in 10 modules covering $-0.41 < \eta < -0.06$. The "start" timing was provided by two identical pseudo-vertex position detectors (pVPD), each 5.4 m away from the TPC center along the beamline [22]. Each pVPD consists of 3 detector elements covering $\sim 19\%$ of the total solid angle in $4.43 < |\eta| < 4.94$ [22].

Since the acceptance of TOFr is small, a special trigger selected events with a valid pVPD coincidence and at least one TOFr hit. A total of 1.89 million and 1.08 million events were used for the analysis from TOFr triggered d+Au and non-single diffractive (NSD) p+p collisions, representing an integrated luminosity of about 40 $\mu$b$^{-1}$ and 30 nb$^{-1}$, respectively.

Minimum-bias d+Au and p+p collisions that did not require pVPD and TOFr hits were also used to study the trigger bias and enhancement, and the TOFr efficiency and acceptance. The d+Au minimum-bias trigger required an equivalent energy deposition of about 15 GeV in the Zero Degree Calorimeter in the Au beam direction [17]. The trigger efficiency was determined to

be $95 \pm 3\%$. Minimum-bias p+p events were triggered by the coincidence of two beam-beam counters (BBC) covering $3.3 < |\eta| < 5.0$ [1]. The NSD cross section was measured to be $30.0 \pm 3.5$ mb by a van der Meer scan and PYTHIA [23] simulation of the BBC acceptance [1]. A small multiplicity bias ( $\lesssim$10% in d+Au and 18% in p+p) at mid-rapidity was observed in TOFr triggered events due to the further pVPD trigger requirement and was corrected for using minimum-bias data sets and PYTHIA [23] and HIJING [24] simulations. The effect of the trigger bias on the mid-rapidity particle spectra was found to be independent of particle $p_T$.

Centrality tagging of d+Au collisions was based on the charged particle multiplicity in $-3.8 < \eta < -2.8$, measured by the Forward Time Projection Chamber in the Au beam direction [17, 25]. The TOFr triggered d+Au events were divided into three centralities: most central 20%, 20−40% and 40− ∼ 100% of the hadronic cross section. The average number of binary collisions $\langle N_{bin} \rangle$ for each centrality class and for the combined minimum-bias event sample is derived from Glauber model calculations and listed in Table I.

The TPC and TOFr are two independent systems. In the analysis, hits from particles traversing the TPC were reconstructed as tracks with well defined geometry, momentum and *dE/dx* [19]. The particle trajectory was then extended outward to the TOFr detector plane. The pad with the largest signal within one pad distance to the projected point was associated with the track for further time-of-flight and velocity ($\beta$) calculations. The time of flight is calculated from the difference between the pVPD start signal and TOFr stop signal. Due to the low multiplicity in d+Au and p+p collisions, the effective timing resolution of the pVPDs was 85 ps and 140 ps, respectively. The average MRPC TOFr timing resolution alone for the ten modules used in this analysis was 85 ps for both d+Au and p+p collisions. Fig. 1 shows $1/\beta$ from TOFr measurement as a function of momentum ($p$) calculated from TPC tracking in TOFr triggered d+Au collisions. Protons/kaons and kaons/pions can be separated by $2\sigma$ up to $p_T \simeq 3$ and $\simeq 1.6$ GeV/c, respectively. In p+p collisions, the corresponding $p_T$ reaches are $\simeq 2$ and $\simeq 1.4$ GeV/c as limited by the pVPD timing resolution. The raw yields of $\pi^{\pm}$, $K^{\pm}$, $p$ and $\bar{p}$ are obtained from Gaussian fits to the distributions in $m^2 = p^2(1/\beta^2 - 1)$ in each $p_T$ bin.

Acceptance and efficiency calculations were done in two independent ways. The first one embedded particles from GEANT into real data to simulate the TPC and TOFr response, track reconstruction in the TPC, and matching between TPC and TOFr. The other method used minimum-bias data to study the TOFr acceptance and matching efficiency, and only used the GEANT simulation to obtain the tracking efficiency in the TPC. The latter one assumed that the TOFr had the same response for $\pi, K$ and $p$ at high $p_T$ where TPC *dE/dx* cannot identify those particles. The results from these two methods were consistent to within 5% in all $p_T$ bins. TPC tracking and MRPC hit matching efficiencies were both about 90%. Weak-decay feeddown (e.g. $K^0_s \rightarrow \pi^+\pi^-$) to pions is ∼ 12% at low $p_T$ and ∼ 5% at high $p_T$, and was corrected for using PYTHIA [23] and HIJING [24] simulations. Inclusive $p$ and $\bar{p}$ production is presented without hyperon feeddown correction. $p$ and $\bar{p}$ from hyperon decays have the same detection efficiency as primary $p$ and $\bar{p}$ [26] and contribute about 20% to the inclusive $p$ and $\bar{p}$ yield, as estimated from the simulation.

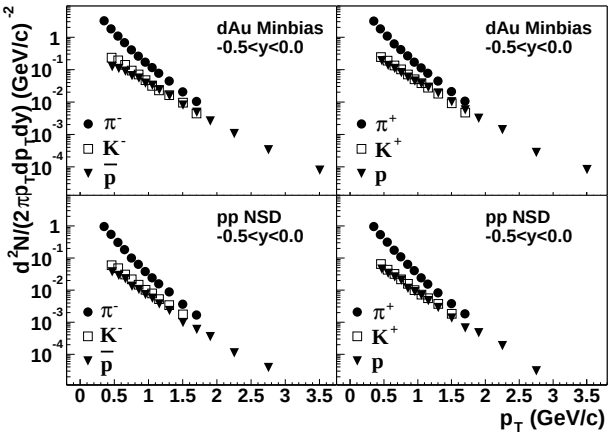


FIG. 2: The invariant yields of pions (filled circles), kaons (open squares), protons (filled triangles) and their antiparticles as a function of $p_T$ from d+Au and NSD p+p events at 200 GeV. The rapidity range was $-0.5 < y < 0.0$ with the direction of the outgoing Au ions as negative rapidity. Errors are statistical.

The invariant yields $d^2N/(2\pi p_T dp_T dy)$ of $\pi^{\pm}$, $K^{\pm}$, $p$ and $\bar{p}$ from both NSD p+p and minimum-bias d+Au events are shown in Fig. 2. The average bin-to-bin systematic uncertainty was estimated to be of the order of 8%. The systematic uncertainty is dominated by the uncertainty in the detector response in Monte Carlo simulations (±7%). Additional factors contributing to the total systematic uncertainty include the background correction (±3%), the small $\eta$ acceptance of the TOFr (±2%), TOFr response (±2%), the correction for energy loss in the detector ($\lesssim 10 \pm 10\%$ at $p_T < 0.6$ GeV/c for the $p$ and $\bar{p}$, much smaller for other species and negligible at higher $p_T$), absorption of $\bar{p}$ in the material (±3%) and the momentum resolution correction ($\simeq 5 \pm 2\%$). The normalization uncertainties in d+Au minimum-bias and p+p NSD collisions are 10% and 14%, respectively [17]. The charged pion yields are consistent with $\pi^0$ yields measured by the PHENIX collaboration in the overlapping $p_T$ range [2, 18].

Nuclear effects on hadron production in d+Au collisions are measured through comparison to the p+p spectrum scaled by the number of underlying nucleon-nucleon

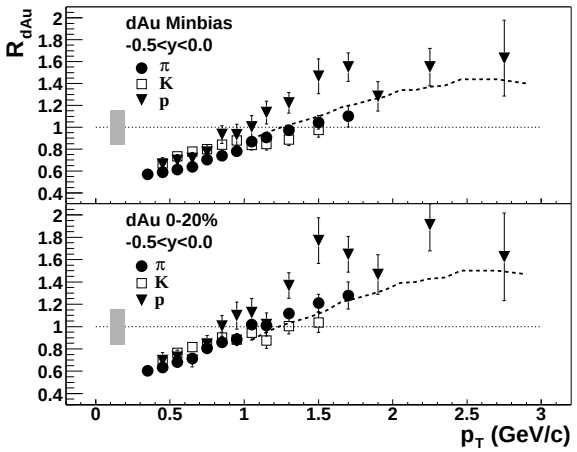


FIG. 3: The identified particle $R_{dAu}$ for minimum-bias and top 20% d+Au collisions. The filled triangles are for $p+\bar{p}$, the filled circles are for $\pi^+ + \pi^-$ and the open squares are for $K^+ + K^-$. Dashed lines are $R_{dAu}$ of inclusive charged hadrons from [17]. Errors are statistical. The gray band represents the normalization uncertainty of 16%.

inelastic collisons using the ratio

$$R_{dAu} = \frac{d^2N/(2\pi p_T dp_T dy)}{T_{dAu} d^2\sigma^{pp}_{inel}/(2\pi p_T dp_T dy)},$$

where $T_{dAu} = \langle N_{bin}\rangle/\sigma^{pp}_{inel}$ describes the nuclear geometry, and $d^2\sigma^{pp}_{inel}/(2\pi p_T dp_T dy)$ for p+p inelastic collisions is derived from the measured p+p NSD cross section. The difference between NSD and inelastic differential cross sections at mid-rapidity, as estimated from PYTHIA [23], is 5% at low $p_T$ and negligible at $p_T > 1.0$ GeV/c. Fig. 3 shows $R_{dAu}$ of $\pi^+ + \pi^-$, $K^+ + K^-$ and $p+\bar{p}$ for minimum-bias and central d+Au collisions. The systematic uncertainties on $R_{dAu}$ are of the order of 16%, dominated by the uncertainty in normalization. The $R_{dAu}$ of the same particle species are similar between minimum-bias and top 20% d+Au collisions. In both cases, the $R_{dAu}$ of protons rise faster than $R_{dAu}$ of pions and kaons. We observe that the spectra of $\pi^{\pm}$, $K^{\pm}$, $p$ and $\bar{p}$ are considerably harder in d+Au than those in p+p collisions.

Fig. 4 depicts $(p+\bar{p})/h$, the ratio of $p+\bar{p}$ over inclusive charged hadrons as a function of $p_T$ in d+Au and p+p minimum-bias collisions at $\sqrt{s_{NN}} = 200$ GeV, and Au+Au minimum-bias collisions at $\sqrt{s_{NN}} = 130$ GeV [5]. The systematic uncertainties on these ratios were estimated to be of the order of 10% for $p_T \lesssim 1.0$ GeV/c, decreasing to 3% at higher $p_T$. At RHIC energies, the anti-particle to particle ratios approach unity ($\bar{p}/p = 0.81 \pm 0.02 \pm 0.04$ in d+Au minimum-bias collisions) and their nuclear modification factors are similar. The $(p+\bar{p})/h$ ratio from minimum-bias Au+Au collisions [5] at a similar energy is about a factor of 2 higher than that in d+Au and p+p collisions for $p_T \gtrsim 2.0$ GeV/c.

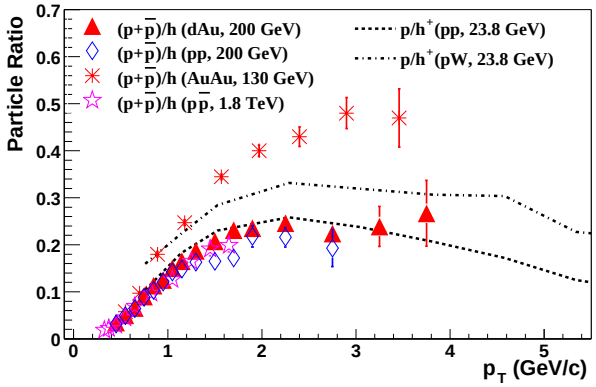


FIG. 4: Minimum-bias ratios of $(p+\bar{p})$ over charged hadrons at $-0.5 < \eta < 0.0$ from $\sqrt{s_{NN}} = 200$ GeV p+p (open diamonds), d+Au (filled triangles) and $\sqrt{s_{NN}} = 130$ GeV Au+Au [5] (asterisks) collisions. Results of $p+\bar{p}$ collisions at $\sqrt{s_{NN}} = 1.8$ TeV [27] are shown as open stars. Dashed lines are results of $p/h^+$ ratios from $\sqrt{s_{NN}} = 23.8$ GeV p+p (short-dashed lines) and p+W (dot-dashed) collisions [12]. Errors are statistical.

TABLE I: $\langle N_{bin}\rangle$ from a Glauber model calculation, $(p+\bar{p})/h$ averaged over the bins within $1.2 < p_T < 2.0$ GeV/c (left column) and within $2.0 < p_T < 3.0$ GeV/c (right column) and the $R_{dAu}$ ratios between $p+\bar{p}$ and $h$ averaged over $1.2 < p_T < 3.0$ GeV/c for minimum-bias, centrality selected d+Au collisions and minimum-bias p+p collisions. A p+p inelastic cross section of $\sigma_{inel} = 42$ mb was used in the calculation. For $R_{dAu}$ ratios, only statistical errors are shown and the systematic uncertainties are 0.03 for all centrality bins.

| centrality | $\langle N_{bin}\rangle$ | $(p+\bar{p})/h$ | | $R^{p+\bar{p}}_{dAu}/R^{h}_{dAu}$ |
|---|---|---|---|---|
| min. bias | $7.5 \pm 0.4$ | $0.21 \pm 0.01$ | $0.24 \pm 0.01$ | $1.19 \pm 0.05$ |
| 0–20% | $15.0 \pm 1.1$ | $0.21 \pm 0.01$ | $0.24 \pm 0.02$ | $1.17 \pm 0.06$ |
| 20–40% | $10.2 \pm 1.0$ | $0.21 \pm 0.01$ | $0.24 \pm 0.02$ | $1.17 \pm 0.06$ |
| 40–∼100% | $4.0^{+0.8}_{-0.3}$ | $0.19 \pm 0.01$ | $0.23 \pm 0.02$ | $1.12 \pm 0.06$ |
| p+p | 1.0 | $0.17 \pm 0.01$ | $0.21 \pm 0.02$ | — |

This enhancement is most likely due to final-state effects in Au+Au collisions [3, 6, 7, 9, 10, 11]. The ratios show little centrality dependence in d+Au collisions, as shown in Table I. For $p_T < 2.0$ GeV/c, the ratio in $p+\bar{p}$ collisions at $\sqrt{s_{NN}} = 1.8$ TeV [27] is very similar to those in d+Au and p+p collisions at $\sqrt{s_{NN}} = 200$ GeV. Also shown are $p/h^+$ ratios in p+p and p+W minimum-bias collisions at $\sqrt{s_{NN}} = 23.8$ GeV [12]. Although the relative yields of particles and anti-particles are very different at $\sqrt{s} < 40$ GeV due to the valence quark effects from target and projectile, the Cronin effects are similar.

The difference between $R_{dAu}$ at $\sqrt{s_{NN}} = 200$ GeV for $p+\bar{p}$ and $h$ can be obtained from the $(p+\bar{p})/h$ ratios in d+Au and p+p collisions. Table I shows $R^{p+\bar{p}}_{dAu}/R^{h}_{dAu}$ determined by averaging over the bins within $1.2 < p_T < 3.0$ GeV/c. At lower energy, the $\alpha$ parameter in the power law dependence on target atomic weight $A^{\alpha}$ of identified particle production falls with $\sqrt{s}$ [12]. From

the ratios of $R_{dAu}$ between $p+\bar{p}$ and $h$, we may further derive the $\alpha_p - \alpha_\pi$ for $1.2 < p_T < 3.0$ GeV/c to be $0.041 \pm 0.010$(stat)$\pm 0.006$(syst) under the assumptions that $\alpha_K \simeq \alpha_\pi$ and that $(p+\bar{p})/\pi$ and $K/\pi$ are between 0.1 and 0.4 in p+p collisions. This result is significantly smaller than the value $0.095 \pm 0.004$ in the same $p_T$ range found at lower energies [12].

In summary, we have reported the identified particle spectra of pions, kaons, and protons at mid-rapidity from 200 GeV p+p and d+Au collisions. The time-of-flight detector, based on novel multi-gap resistive plate chamber technology, was used for particle identification. The timing resolution of the MRPC was 85 ps. The particle-species dependence of the Cronin effect is found to be significantly smaller than that from lower energy p+A collisions. In $\sqrt{s_{NN}} = 200$ GeV d+Au collisions, the ratio of the nuclear modification factor $R_{dAu}$ between $(p+\bar{p})$ and charged hadrons $(h)$ in the $p_T$ range $1.2 < p_T < 3.0$ GeV/c was measured to be $1.19 \pm 0.05$(stat)$\pm 0.03$(syst) in minimum-bias collisions and shows little centrality dependence. The ratios of protons over charged hadrons in d+Au and p+p collisions are found to be about a factor of 2 lower than that from Au+Au collisions, indicating that the Cronin effect alone is not enough to account for the relative baryon enhancement observed in heavy ion collisions.

The Star Collaboration gratefully acknowledges the pioneering research and development work performed by LAA project, and especially C. Williams, under A. Zichichi on MRPC Time of Flight Technology. We thank the RHIC Operations Group and RCF at BNL, and the NERSC Center at LBNL for their support. This work was supported in part by the HENP Divisions of the Office of Science of the U.S. DOE; the U.S. NSF; the BMBF of Germany; IN2P3, RA, RPL, and EMN of France; EPSRC of the United Kingdom; FAPESP of Brazil; the Russian Ministry of Science and Technology; the Ministry of Education and the NNSFC of China; SFOM of the Czech Republic, DAE, DST, and CSIR of the Government of India; the Swiss NSF.

[1] STAR Collaboration, J. Adams *et al.*, nucl-ex/0305015.
[2] PHENIX Collaboration, S.S. Adler *et al.*, Phys. Rev. Lett. **91**, 072301 (2003); PHENIX collaboration, S.S. Adler *et al.*, hep-ex/0304038.
[3] M. Gyulassy *et al.*, nucl-th/0302077.
[4] STAR Collaboration, J. Adams *et al.*, nucl-ex/0306007.
[5] PHENIX Collaboration, K. Adcox *et al.*, Phys. Lett. B **561**, 82 (2003); PHENIX Collaboration, S.S. Adler *et al.*, nucl-ex/0305036.
[6] D. Teaney *et al.*, nucl-th/0110037; D. Teaney *et al.*, Phys. Rev. Lett. **86**, 4783 (2001).
[7] P. Huovinen, Nucl. Phys. A **715**, 299c (2003).
[8] R.C. Hwa *et al.*, Phys. Rev. C **67**, 034902 (2003).
[9] R.J. Fries *et al.*, nucl-th/0306027.
[10] V. Greco *et al.*, Phys. Rev. Lett. **90**, 202302 (2003).
[11] I. Vitev and M. Gyulassy, Phys. Rev. C **65**, 041902 (2002).
[12] J.W. Cronin *et al.*, Phys. Rev. Lett. **31**, 1426 (1973); J.W. Cronin *et al.*, Phys. Rev. D **11**, 3105 (1975); D. Antreasyan *et al.*, Phys. Rev. D **19**, 764 (1979); P.B. Straub *et al.*, Phys. Rev. Lett. **68**, 452 (1992).
[13] M. Lev and B. Petersson, Z. Phys. C **21**, 155(1983).
[14] A. Accardi, hep-ph/0212148, (2002); X.N. Wang, Phys. Rev. C **61**, 064910 (2000).
[15] T. Alexopoulos *et al.*, Phys. Lett. B **435**, 453 (1998).
[16] D. Kharzeev *et al.*, Phys. Lett. B **561**, 93 (2003); D. Kharzeev *et al.*, hep-ph/0307037; R. Baier *et al.*, hep-ph/0305265.
[17] STAR Collaboration, J. Adams *et al.*, Phys. Rev. Lett. **91**, 072304 (2003).
[18] PHENIX Collaboration, S.S. Adler *et al.*, Phys. Rev. Lett. **91**, 072303 (2003); PHOBOS Collaboration, B.B. Back *et al.*, Phys. Rev. Lett. **91**, 072302 (2003); BRAHMS Collaboration, I. Arsene *et al.*, Phys. Rev. Lett. **91**, 072305 (2003).
[19] M. Anderson *et al.*, Nucl. Instr. Meth. A **499**, 659 (2003).
[20] B. Bonner *et al.*, Nucl. Instr. Meth. A **508**, 181 (2003); M. Shao *et al.*, Nucl. Instr. Meth. A **492**, 344 (2002).
[21] E. Cerron Zeballos *et al.*, Nucl. Instr. Meth. A **374**, 132 (1996); M.C.S. Williams *et al.*, Nucl. Instr. Meth. A **478**, 183 (2002).
[22] W.J. Llope *et al.*, nucl-ex/0308022.
[23] T. Sjöstrand, P. Eden, C. Friberg *et al.*, Comput. Phys. Commun. **135**, 238 (2001).
[24] X.N. Wang and M. Gyulassy, Phys. Rev. D **44**, 3501 (1991).
[25] K.H. Ackermann *et al.*, Nucl. Instr. Meth. A **499**, 713 (2003).
[26] STAR Collaboration, C. Adler *et al.*, Phys. Rev. Lett. **87**, 262302 (2001).
[27] T. Alexopoulos *et al.*, Phys. Rev. D **48**, 984 (1993).